TDA Progress Report 42-101

May 15, 1990

Goldstone Intracomplex Connected Element Interferometry

C. D. Edwards
Tracking Systems and Applications Section

Interferometric observations of the radio source pair 3C 84 and OE 400 have been made on the 21-km baseline between DSS 13 and DSS 15 to explore the angular navigation potential of intracomplex connected element interferometry (CEI). The differential phase-delay observable formed from pairs of 3-minute scans exhibited a precision of 1 psec, while the actual scatter of the phase-delay residuals for eleven scans over the 90-minute observing session was about 10 psec, consistent with the expected few-millimeter fluctuations in the wet tropospheric path delay. Fitting for the position of OE 400 relative to 3C 84 yielded an error ellipse with a semi-minor axis of 60 nrad. Given the short data arc in this experiment, the orthogonal direction in the plane of the sky is not well determined; however, a second baseline or a data arc spanning a larger fraction of the source mutual visibility window could provide simultaneous determination of both right ascension and declination. Examination of the phase-delay residuals supports the accuracy of the cycle ambiguity resolution. However, reliable phase ambiguity resolution will pose the most significant challenge to routine use of CEI for spacecraft tracking, particularly when the a priori spacecraft source position is not well known. Several approaches for ambiguity resolution are briefly outlined.

I. Introduction

Connected element interferometry (CEI) can provide accurate angular tracking from short intracomplex baselines by making use of the very precise phase-delay data type. A number of operational advantages result from being able to form the angular tracking observable from data collected within a single Deep Space Communications Complex (DSCC), including the potential for real-time data processing and fringe verification, as well as near-real-time delivery of tracking observables to the orbit determination navigation software. Some of the motivations for CEI are discussed in [1]. Previous intracomplex observations at Goldstone on the 6-km baseline between DSS 13 and DSS 12 have been reported [1,2].

CEI could provide an efficient angular tracking capability during mission phases where the full precision of intercontinental very long baseline interferometry (VLBI) is not required. A 50–100 nrad intracomplex angular tracking capability on baselines of 20 km would represent an improvement over the current few-hundred-nrad angular accuracy of Doppler tracking. In addition, the CEI observable would not require long, continuous data arcs

and would not suffer from the well-known singularity of the Doppler data type near zero declination. Increasing the CEI baseline lengths to 100 km could further improve angular accuracy to the 10–20 nrad level. Intercontinental VLBI would still provide the highest angular capabilities for specific mission requirements. Current VLBI accuracy is at the 30–50 nrad level for the operational Block I VLBI system,[1] while future systems may deliver nanoradian-level accuracy relative to the quasar frame [3] and 10-prad accuracy for relative angular tracking of two or more spacecraft within the same primary antenna beam [4].

In this article, the first set of differential phase-delay observations on the 21-km baseline between DSS 13 and DSS 15 is presented. This is the longest baseline currently available within any of the DSCCs. DSS 13 is the Deep Space Network (DSN) Advanced Systems Program's 26-m research and development antenna, while DSS 15 is a high-efficiency, 34-m antenna used primarily for operational DSN spacecraft tracking. Differential spacecraft-quasar observations have been simulated by observing a pair of quasars, 3C 84 and OE 400, separated by 6 deg in the plane of the sky. After describing the observing schedule and the data acquisition system, the observable formation will be reviewed. The resulting differential phase-delay residuals will be examined in light of previously reported calculations which suggest that tropospheric fluctuations should dominate the CEI differential phase observable [5].

Weighting the data to reflect the observed scatter, the differential phase-delay residuals will be used to solve for the relative positions of the two quasars. The resulting source position error ellipse characterizes the angular information content of this intracomplex CEI pass. Since the a priori relative source positions are well known and based on many years of high-accuracy VLBI observations, the size of the estimated relative position shift also serves as a consistency check on the CEI results.

Finally, potential problems relating to reliable ambiguity resolution will be discussed, along with a brief outline of several alternative approaches to ambiguity resolution.

II. Experiment Description

Previous intracomplex phase-delay observations at Goldstone have been made on the 6-km baseline between DSS 12 and DSS 13, using a fiber-optic link between those stations to operate them coherently [1,2]. These observations were encouraging in that phase connection was reliably achieved and the final phase-delay residuals were just a few millimeters, but the extremely short baseline limited the angular resolution of these observations to many hundreds of nrad. When the fiber-optic link at Goldstone was extended to SPC-10, where both DSS 14 and DSS 15 are located, a 21-km baseline between DSS 13 and the SPC-10 antennas became available. This longer baseline offers the potential for much greater angular accuracy. With the goals of understanding the limiting phase-delay errors, demonstrating phase ambiguity resolution, and quantifying the angular accuracy on this 21-km baseline, an experiment was planned and scheduled.

Interferometric data were acquired on May 27, 1988, from 2130–2300 UT, at DSS 13 and DSS 15 in the Goldstone DSCC. Observations were made at both 2.3 GHz (S-band) and 8.4 GHz (X-band) to allow calibration of the effects of charged particles. A hydrogen maser at SPC-10 provided the frequency reference for DSS 15; the analog fiber-optic link was used to transfer this frequency reference to DSS 13, allowing the two stations to be operated coherently. Previously reported tests of the fiber-optic link indicate that the link stability $\Delta\nu/\nu$ is well below 10^{-14} for averaging times of several hundred seconds [6].

The Block 0 VLBI data acquisition system was used to single-bit quantize, sample, format, and record the incoming signals at each station [7]. The Block 0 system records a single 2-MHz baseband signal, sampled with 1-bit quantization at the Nyquist rate, resulting in a 4-Mbit/sec data rate. This 2-MHz bandwidth was time-multiplexed over six separate sky frequencies, three at S-band and three at X-band. Each S-band channel was observed for 0.4 sec, while each X-band channel was observed for 1.6 sec, during each 6-second multiplexing cycle. (The longer X-band dwells were chosen because the X-band observable carries a greater weight in the final S/X linear combination.)

A. Frequency Constraints on Short Baselines

Table 1 shows the sky frequencies and channel dwell times used in this experiment. Note the 200-Hz offset between the local oscillator (LO) frequencies at the two stations. This is required due to the small differential Doppler shift between stations, and can be understood as follows: The sidereal rotation of the Earth induces a Doppler shift, for observations in the direction of a given radio source, at each station of an interferometer. For short baseline observations, the differential Doppler shift ν_D between the two stations becomes very small, typically less than 10 Hz

[1] J. B. Thomas, "An Error Analysis for Galileo Angular Position Measurements with the Block I ΔDOR System," JPL Engineering Memorandum 335-26 (internal document), Jet Propulsion Laboratory, Pasadena, California, November 11, 1981.

at 2.3 GHz on a 21-km baseline. Adding a local oscillator offset ν_{OFF} ensures that when the signals from the two stations are cross-correlated (i.e., multiplied), the resulting fringe frequency, $\nu_F = \nu_D + \nu_{OFF}$, will be well separated from dc. When the fringes are subsequently counter-rotated, or "stopped," by multiplying them with a model sinusoid with frequency $\tilde{\nu}_F \approx \nu_F$, both sum and difference frequencies are generated, at roughly $2\nu_F$ and 0, respectively. In the subsequent coherent integration, the high-frequency term will be attenuated if the integration time $\tau \gg 1/(2\nu_F)$, leaving only the stopped fringe phase, as desired. With the coherent integration time of 0.2 sec used at the correlator, the 200-Hz LO shift ensures that this is the case.

Phase calibration tones were injected at each station at both S-band and X-band frequencies to calibrate temporal fluctuations in the instrumental phase. Here again, some modifications to standard VLBI procedure were required due to the short baselines. If the same calibration tone frequencies are used at both stations, the cross-correlation of these phase calibration tones will produce a signal with very nearly the same frequency as the actual quasar fringes, even when an LO offset is used, due to the very small differential Doppler shift between stations on a short baseline. For this reason, different calibration tone frequencies were used at each station in this experiment. The DSN phase calibration system produces calibration tones at integral multiples of $5/N$ MHz, where N is user-selectable in the range 5–99. A value of $N = 7$ was used for DSS 13, and $N = 8$ for DSS 15. This choice placed at least three calibration tones in each 2-MHz channel. All tones in each channel were phase-tracked and used during the correlation process to calibrate instrumental phase errors.

B. Observations and Initial Processing

The experiment observing schedule consisted of repeated differential observations of the two radio sources 3C 84 and OE 400. These sources are separated by about 6 degrees in the plane of the sky. Table 2 summarizes the a priori J2000 positions of the two sources, based on many years of DSN VLBI observations. Each source was observed for 180 sec, with a slew time of 30–45 sec between observations. Both sources were setting during the period of observation; 3C 84 varied in elevation from 57° down to 42°, while OE 400 varied from 53° down to 40°. (On the DSS 13–DSS 15 baseline, the elevation angles at the two stations will always agree to 0.2 deg or better.) Table 3 lists the sequence of observations. One observation pair was lost due to a brief failure of the DSS 13 antenna pointing computer at 215945 GMT. All other scans were successful.

The recorded data, on Block 0 VLBI videocassettes, were processed at the JPL/Caltech Block II VLBI correlator [8]. The output of this initial processing is sine and cosine correlation sums for each of the six channels at a rate of one point per channel every six seconds, corresponding to the time-multiplexing cycle period. These correlation sums were then processed with the REVERT/PHASOR software package to fit for fringe amplitude and phase for each channel. Fringes were obtained for all of the observations for which data were obtained.

With three frequency channels recorded at S-band and three at X-band, it is possible to form group delay observables using the bandwidth synthesis (BWS) technique [9]. Although not a goal of this experiment, the BWS observable was formed as a check on the quality of the data. The BWS observable is formed by calculating the slope of phase versus frequency over a given spanned bandwidth:

$$\tau_{BWS} = \frac{\phi(\nu_1) - \phi(\nu_2)}{\nu_1 - \nu_2}$$

For the channel frequencies used in this experiment, the maximum spanned bandwidth $\nu_1 - \nu_2$ was 40 MHz at both S-band and X-band. The formal error on the X-band BWS delay observable was about 100 psec for 3C 84, and over 200 psec for OE 400, with somewhat higher errors at S-band due to the shorter dwell times. These errors correspond to path-delay errors on the order of 5 cm, or angular errors of several μrad on a 21-km baseline.

III. The Phase Observable and Ambiguity Resolution

To achieve angular accuracies of better than 100 nrad, the much more precise phase data type is required. The geometric component of the interferometric phase can best be thought of as a measure of the geometric delay in units of the observing wavelength. To make use of the interferometric phase, however, one must be able to resolve the integer cycle ambiguity associated with that data type. Further complicating the ambiguity resolution is the contribution of nongeometric errors to the phase, such as the unknown LO phase offset between stations, propagation media delays, and unknown instrumental delays and dispersions.

In principle, the BWS delay residuals contain information about errors in the correlator delay model that could be used to resolve the phase observable on a scan-by-scan basis. However, the formal errors on the BWS delay residuals in this experiment were on the order of an RF cycle (120 psec at X-band) or larger, and thus could

not be used to aid in ambiguity resolution. (It should be pointed out, however, that a wider BWS spanned bandwidth coupled with a larger total recorded bandwidth could provide sufficient BWS precision to enable cycle ambiguity resolution for each scan based on the BWS residual. This more robust approach to ambiguity resolution will be attempted in an experiment planned for early 1990 on this same baseline, using the wider bandwidth Block II VLBI system, which is capable of providing 10-psec BWS precision.)

Instead, for this experiment it was necessary to determine an a priori delay model which was accurate enough to resolve the cycle ambiguity directly. Using the MASTERFIT VLBI parameter estimation software [10] and the best a priori models for station locations and source positions, an (ambiguous) residual phase observable was calculated for each quasar observation. Consider observations of two sources, A and B, and let ϕ_A represent the total phase observable for source A, N_A the unknown integer cycle ambiguity, ω_{RF} the RF observing frequency, and $\tilde{\tau}_A$ the a priori model delay. Then the phase residual $\widehat{\phi}_A$ can be written

$$\widehat{\phi}_A = \phi_A + 2\pi N_A - \omega_{RF}\tilde{\tau}_A$$

A similar phase residual can be formed for the subsequent observation of source B:

$$\widehat{\phi}_B = \phi_B + 2\pi N_B - \omega_{RF}\tilde{\tau}_B$$

If the a priori model were sufficiently accurate, the integer cycle ambiguities N_A and N_B could each be determined by the requirement that the phase residuals be near zero. However, the above-mentioned nongeometric model uncertainties are typically on the order of an RF cycle or more, generally preventing this.

By differencing the two phase observations, many of the model uncertainties are canceled or reduced, thereby allowing the determination of the *relative* cycle ambiguity $N_A - N_B$. Forming a differential observable yields

$$\begin{aligned}\Delta\widehat{\phi}_{A-B} &= (\phi_A - \phi_B) + 2\pi(N_A - N_B) - \omega_{RF}(\tilde{\tau}_A - \tilde{\tau}_B) \\ &\equiv \Delta\phi_{A-B} + 2\pi\Delta N_{A-B} - \omega_{RF}\Delta\tilde{\tau}_{A-B}\end{aligned}$$

Many potential error sources in the delay models $\tilde{\tau}$ are reduced or eliminated by this differencing. The unknown offset of the LO phases between the two stations, which manifests itself as a clock offset for the single-source observable, cancels completely in the differential observable. Geometric errors are also largely reduced by differencing the phase delays for angularly close sources. A baseline uncertainty of size ΔB can cause an error of up to $\Delta B/c$ in the delay model for an individual source, where c is the speed of light. However, when two sources with a small angular separation of $\Delta\theta$ are differenced, much of this geometric error cancels. The resulting error in the differenced model delay will be bounded by $\Delta B\Delta\theta/c$, where $\Delta\theta$ is expressed in radians. For example, a 6-deg angular source separation will cause geometric model errors to be reduced by about a factor of 10 in a differential observable. Thus even a 2-cm baseline error, representing a full half-cycle error for X-band observations, would be reduced to a 2-mm maximum path-delay error for a differential observable between sources separated by 6 deg, and would not complicate the relative phase connection.

Similarly, propagation media errors are greatly reduced by differencing observables for angularly close sources. Any uncertainty in the overall tropospheric delay at each station is greatly attenuated due to several factors: The short baseline causes the total zenith delays at the two stations to be highly correlated; the short baseline also causes the two stations to observe a source at nearly the same elevation angle; and the angular proximity of the sources also causes the elevation angles for the two sources to be nearly the same at each station. The remaining error is predominantly due to small-scale temporal and spatial fluctuations in the tropospheric delay, on the time scale of the time between scans, and on the spatial scale of the angular distance between sources, projected to the tropospheric scale height of several kilometers.

The relative cycle ambiguity ΔN is given by

$$\Delta N = \text{nint}\left(\frac{\omega_{RF}\Delta\tilde{\tau} - \Delta\phi}{2\pi}\right)$$

where nint is the "nearest integer" function, and where the subscript $A - B$ has been dropped. The reliability of the phase ambiguity determination is reflected in the size of the final phase residuals. By the above choice of ΔN, the residuals will lie between $\pm 1/2$ cycle; for the phase connection to be deemed reliable, however, the residuals should be distributed in a peak around zero and be well separated from $\pm 1/2$ cycle.

For this condition to be satisfied, two criteria must be met: both the precision of the differential phase observable $\Delta\phi$ and the error in the a priori differential model delay $\Delta\tilde{\tau}$ must be well below 1/2 cycle of phase. The first criterion is usually satisfied just by the requirement that the sources be detected with good SNR since the statistical phase error, expressed in radians, is roughly 1/SNR.

The second criterion is more difficult to ensure. Given known uncertainties in station location and source position, the geometric component of $\Delta\tilde{\tau}$ can be calculated reliably. However, contributions of unmodeled errors, such as stochastic troposphere fluctuations or antenna deformation, are more difficult to estimate. The approach in this article is to simply determine the phase connection using the best a priori information, and then evaluate the reliability of the phase connection by examining the distribution of phase residuals $\Delta\hat{\phi}$.

Figure 1 shows histograms of the S-band and X-band phase residuals after ambiguity resolution. The residuals show a very clear clustering about zero, with a root-mean-square (rms) value below 1/10th of a cycle for both bands. Quantitatively determining the reliability of the ambiguity resolution requires some assumption about the underlying probability distribution of the phase residual error sources. If it were assumed that the phase residual error was due to a Gaussian error source with a standard deviation of 0.1 cycle, then it would be possible to calculate the likelihood that all of the integer cycle ambiguities had been correctly resolved. The probability that a single observation was correctly resolved would simply be the probability that the observation's phase error was less than 0.5 cycle. For the case of $\sigma = 0.1$ cycle, this is just the integrated Gaussian probability distribution out to $\pm 5\ \sigma$, equal to 0.9999994. For the eleven observations, this gives a cumulative probability of 0.999993 that all eleven observations have been correctly resolved, if it is assumed that the observations are uncorrelated. Unfortunately, the error sources contributing to the observed phase residuals most likely have significant nonGaussian tails that would drastically change this conclusion, increasing the probability of an incorrect integer cycle determination. Obtaining a better characterization of the probability distribution of phase errors, and thus determining more realistically the reliability of cycle ambiguity resolution, is a primary motivation for collecting a much larger database of observations on this intracomplex baseline. At this time, all that can be said is that the distribution of phase residuals after ambiguity resolution strongly suggests that the phase ambiguity resolution was successful for this experiment.

In the final stage of observable formation, the S-band and X-band phase residuals are linearly combined to form an S/X residual phase-delay observable, free from the dispersive effects of charged particles:

$$\Delta\hat{\tau}_{S/X} = \left(\frac{\omega_X^2}{\omega_X^2 - \omega_S^2}\right)\frac{\Delta\hat{\phi}_X}{\omega_X} - \left(\frac{\omega_S^2}{\omega_X^2 - \omega_S^2}\right)\frac{\Delta\hat{\phi}_S}{\omega_S}$$

Figure 2 shows the S/X-corrected differential phase-delay residuals as a function of time for the eleven source pair observations. The rms value of the residuals is 10 psec, or about 3 mm of path delay. The formal statistical error on each point is only about 1 psec; the observed scatter is expected to be due primarily to stochastic spatial and temporal fluctuations of the wet tropospheric path delay at each station. To account for these tropospheric fluctuations, the actual error bars shown on the data points have been inflated to yield a reduced χ^2 equal to 1, as described in Section IV. A previous article [5] calculated the size of such fluctuations and their impact on differential phase-delay observations in CEI, based on numerical integrations of a Kolmogorov turbulence model for atmospheric fluctuations [11]. Using the model described in that article and the relevant parameters of these observations (namely, a 21-km baseline, 6-deg source separation, 3-minute scan and 40-sec slew time, and the range of elevation angles occurring during this experiment) the expected scatter in the differential phase delay is calculated to range from 3.5 to 4.2 mm over the observation period, increasing as the sources set in elevation. The model has some uncertainty due to daily variations in the wind speed and scale height of the wet troposphere. Nonetheless, this excellent level of agreement supports the hypothesis that tropospheric effects are indeed a dominant error source for the CEI differential phase observable.

IV. Relative Source Position Accuracy

The most direct way of demonstrating the angular accuracy of these observations is to solve for the relative angular positions of the two sources, just as one would solve for a spacecraft position relative to a reference quasar. Doing this, one obtains an estimated position correction for one of the quasars, along with a covariance describing the uncertainty in that estimated position. The a priori source positions of both sources in this experiment are known to an accuracy of about 10 nrad, based on many years of observations on long baselines. Thus a consistency check on the estimated position is that it agree, to within the estimated covariance, with the a priori position.

(There may be concern that structure in the radio source brightness distribution could cause the apparent source position to differ on long versus short baselines. Although source structure issues will not be addressed in this article, future CEI observations of a number of source pairs would provide a data set for quantifying this effect. If long- and short-baseline apparent source positions differed significantly, it would be necessary to develop a distinct CEI source position catalog based solely on short-baseline observations.)

The MASTERFIT VLBI software was again used, in this case to estimate a position correction to the source OE 400. As mentioned earlier, the formal statistical errors on the phase-delay data points are only about 1 psec, while the actual scatter of 10 psec is consistent with the expected level of tropospheric fluctuations. To take this into account, an error contribution of about 10 psec was added in quadrature to each differential observation's formal error to obtain the final data weight used in the source position parameter estimation. The size of this supplemental error contribution was determined by requiring the reduced χ^2 of the final fit to equal one. In this way, the actual level of fluctuations observed in the data can be incorporated into the data weights and thereby into the uncertainty in the final source position determination. Given that atmospheric dynamics can vary significantly from day to day, this approach is probably more robust and reliable than trying to specify the data weights based solely on some model of tropospheric fluctuations. Nonetheless, as described earlier, this supplemental phase-delay error contribution, determined empirically, agrees fairly well with the predictions of a statistical model of tropospheric fluctuations.

Using these empirically determined data weights, the eleven differential phase-delay residuals served as input to a weighted least-squares adjustment of the right ascension and declination of OE 400. No other parameters were estimated in this process. The OE 400 source position was essentially unconstrained: the a priori right ascension and declination uncertainties were set at 1 radian. Figure 3 shows the resulting 1-σ error ellipse for the estimated OE 400 position correction. The vertical axis is the declination shift $\Delta\delta$, while the horizontal axis represents the right ascension shift expressed as an arclength: $\Delta\alpha \times \cos\delta$. The error ellipse is very elongated, with a semi-major axis of about 1165 nrad, due to the short data arc. However, in the direction of the average baseline projection during the experiment, the semi-minor axis is 60 nrad. In addition, the 1-σ error ellipse is consistent with the a priori source position, which in this experiment was well known.

These results represent the first time that angular measurements from a single DSN complex have provided accuracies below 100 nrad. The high eccentricity of $\epsilon = 0.90$ for the error ellipse derived from this data set reflects the short span of data. Each single phase-delay observation only contains information for one direction in the plane of the sky, namely, along the projection of the interferometer baseline in the radio source direction. Over the 90-minute duration of this experiment, the baseline projection in the direction toward OE 400 rotates only a small amount, about 10°. Because the experiment duration was so short, the full range of baseline orientation was not sampled, and thus the resulting source position will have a much better determination in one direction—namely, the projected baseline direction at the central epoch of the experiment, with a much larger uncertainty in the orthogonal direction.

To illustrate this, Fig. 4 shows the east–west and north–south components of the projected DSS 13–DSS 15 baseline in the direction of OE 400, over the full 15.5-hour mutual visibility window of this northern declination source. (This can be thought of as the baseline length and orientation, as viewed from the quasar.) The 90-minute observation period represented by the current data set is indicated by the heavy line. The limited range of baseline orientation during the 90-minute observation period underlies the large eccentricity of the estimated OE 400 position error ellipse in this experiment. But over the entire mutual visibility window, the baseline rotates through well over 90°, and hence CEI observations spanning this entire period would provide strong solutions for both components of sky position. Previous analyses[2,3] have shown that CEI observations at Goldstone on the DSS 13–DSS 15 baseline, collected throughout the mutual visibility period, can provide good determination of both α and δ for northern declination sources.

Adding a second baseline, orthogonal to the DSS 13–DSS 15 baseline, would also enable good determination of both components of sky position. This solution has the added advantage that both components could be determined simultaneously from observations taken at a single epoch, instead of combining observations that are separated by many hours—an important advantage in the case of tracking a spacecraft with a poorly determined orbit.

V. Reliability of Ambiguity Resolution

Successful cycle ambiguity resolution is the key to unlocking the high precision of the phase data type. Much more work needs to be done to understand the reliability of ambiguity resolution as a function of baseline length, angular source separation, elevation angle, and temporal scan separation. Nonetheless, one encouraging conclusion

[2] M. H. Finger and C. D. Edwards, "Relative CEI Navigation Performance of Goldstone Intracomplex Baselines," JPL Interoffice Memorandum 335.3-88-116 (internal document), Jet Propulsion Laboratory, Pasadena, California, October 20, 1988.

[3] S. W. Thurman, "Information Content of a Single Pass of Phase-Delay Data From a Short Baseline Connected Element Interferometer," JPL Engineering Memorandum 314-479 (internal document), Jet Propulsion Laboratory, Pasadena, California, December 13, 1989.

of this analysis is that differential phase-delay errors do not seem to grow linearly with baseline length. Limited data on a 6-km, a 21-km, and a 253-km baseline are now available, and in each case, the final delay residual scatter has been at about the 10-psec level. This is consistent with the hypothesis that the scatter is dominated at each site by rapid temporal fluctuations, which are uncorrelated between stations on the short time scale of a differential observation, and therefore are independent of baseline length. In each of these experiments, the a priori source positions were well known; thus the ambiguity resolution was only limited by the size of unmodeled components of the differential delay, particularly these rapid tropospheric fluctuations. At S-band and X-band, this 10-psec level of unmodeled phase-delay uncertainty does not prevent ambiguity resolution. However, at 32 GHz (Ka-band), the delay ambiguity is only about 30 psec. These same errors would then represent a much larger fraction of an RF cycle, seriously complicating phase connection.

Ambiguity resolution also becomes more difficult when the a priori source position of one of the sources is less well known. In the "direct" ambiguity resolution strategy used in this article, in which the integer cycle ambiguity is determined solely on the a priori delay model, one clearly must know the source position in the projected baseline direction to better than half of a fringe spacing. On a 21-km baseline, the minimum fringe spacing is 6.2 μrad at 2.3 GHz and 1.7 μrad at 8.4 GHz. Doppler tracking can usually determine a spacecraft ephemeris with sufficient accuracy to satisfy this constraint during periods of cruise. However, at encounter or during other periods of high spacecraft dynamics, this constraint may be more difficult to satisfy.

Several approaches can be used to improve the reliability of ambiguity resolution in the case that the a priori model delay error is too large to allow "direct" ambiguity resolution. All of them involve starting with a lower accuracy data type, but one whose cycle ambiguity can be reliably resolved. The information in this lower accuracy observable is then used to assist in resolving the cycle ambiguity associated with the higher accuracy data type. Some of these approaches have been discussed previously and are outlined below.[4] What follows is a sketch of possible techniques; more work is required to fully analyze and explore how each of them would perform in an operational CEI system.

[4] S. Thurman, "Continuation of the Connected Element Interferometry System Study," JPL Interoffice Memorandum 314.5-1367 (internal document), Jet Propulsion Laboratory, Pasadena, California, October 20, 1988.

A. BWS Aiding

As mentioned previously, with sufficient spanned bandwidth, BWS group delay residuals can be determined with formal errors of less than a cycle of RF phase. In that case, if dispersive errors can be accurately calibrated and removed, the group delay residual can be used to correct the delay model and aid in ambiguity resolution. How precise must the BWS observable be to aid in ambiguity resolution? Consider a system with two BWS channels, separated in frequency by a spanned bandwidth of ν_{BWS}, and with a formal phase error of σ_ϕ cycles. Requiring that the BWS observable precision be less than 1/6th of an RF cycle, to ensure reliable ambiguity resolution, yields:

$$\frac{\sqrt{2}\sigma_\phi}{\nu_{BWS}} < \frac{1}{6\nu_{RF}}$$

With a 400-MHz spanned bandwidth and a 5-mcyc phase error in each channel, it would then be possible to resolve RF cycles at X-band. It is important to keep in mind that this argument has ignored the effects of dispersive errors due to the ionosphere, solar plasma, or instrumentation, which contribute differently to the phase and group delay data types.

For use in spacecraft tracking, this technique of BWS-aided ambiguity resolution will require large spanned bandwidths on the spacecraft. However, the current X-band deep space downlink frequency allocation is only 40 MHz wide, probably insufficient for resolving the X-band or even the S-band phase ambiguity. At Ka-band, however, a full 500-MHz downlink allocation exists and could aid ambiguity resolution. For example, with a spacecraft incorporating a dual-band X/Ka downlink, and with widely spaced VLBI tones at Ka-band, the accurate Ka-band BWS observable could be used to resolve the X-band phase observable. Such a scenario has been proposed for same-beamwidth interferometric tracking of two spacecraft at Mars with simultaneous X/Ka downlinks [12].

B. Band-to-Band Aiding

Just as one can "step" from the BWS observable, with its spanned bandwidth ν_{BWS}, up to the phase observable at frequency ν_{RF}, one can also imagine using the phase observable at a lower frequency band to aid the phase ambiguity resolution at a higher frequency band, e.g., using an S-band phase residual to resolve the X-band phase ambiguity. Again, the key to making this work is the requirement that dispersive errors represent much less than a cycle of phase at the higher frequency. Instrumental phase calibrations can probably reduce instrumental dispersion to a

few degrees of phase, in which case they would not pose an obstacle to stepping from one band to the next. In that case, the biggest dispersive error will be due to the effects of charged particles in the ionosphere and solar plasma. Since charged-particle delays scale as $1/\nu^2$, whereas cycle ambiguities scale as $1/\nu$, charged particles will represent a four times more serious error in stepping from S-band to X-band than in stepping from X-band to Ka-band.

The current understanding of ionospheric errors and, in particular, spatial and temporal fluctuations in ionospheric delays is not as well developed as the corresponding understanding of tropospheric errors. Empirically, however, the concept of S-to-X-band aiding in the current data set can be tested by asking the question: if the final S-band phase delays had been used instead of the a priori delay model to resolve the X-band phase, would the same integer cycle ambiguities have been determined? Examining the S-band phase delay residuals, it was found that ten of the eleven X-band observables would have been resolved identically. However, one observation (the outlier in the S-band histogram of Fig. 1) would have had a 1-cycle shift in the final X-band observable. Presumably the "direct" solution in this case is the correct one, not the "S-to-X-aided" solution, based on the final distribution of X-band residuals for the repeated observations of the source pair. It is not known whether the S-band outlier was caused by an uncalibrated instrumental fluctuation or by actual fluctuations in the ionosphere above Goldstone.

C. Baseline Aiding

Going to shorter baselines increases the fringe spacing on the sky, and thus relaxes the a priori source position requirements for phase connection (at the cost of lower angular precision). One can imagine a series of progressively longer baselines, where the phase residual on each baseline would be used to aid the ambiguity resolution of the next longer baseline. If the a priori position knowledge is sufficient to resolve the phase ambiguity on the shortest baseline, and if each baseline's phase-delay residual is sufficiently accurate to resolve the ambiguity on the next longer baseline, then ultimately the phase ambiguity on the longest baseline can be resolved. This technique works best if the baselines are exactly parallel, since each baseline only measures instantaneously one component of the source position.

Consider a linear array of five antennas with coordinates of 0, 1, 5, 25, and 125 km along some line. At X-band, the 1-km baseline formed by the first two antennas would correspond to a very large minimum fringe spacing of 40 μrad. Phase connection on this baseline would require only very crude a priori source position information. If the phase observable on this 1-km baseline were sufficient to determine the source position (along the projected baseline direction) to a 1-σ uncertainty of 1/30th of a fringe spacing, that improved source position would enable reliable ambiguity resolution on the 5-km baseline, i.e., the 3-σ source position error would contribute less than half a cycle of phase on the 5-km baseline. This process would continue until the 125-km baseline was reached. A 1/30th of a cycle error on the 125-km baseline would correspond to a 10-nrad angular position determination at X-band.

Each of these techniques has inherent strengths and weaknesses in terms of requirements of the CEI system. The BWS or band-to-band techniques could help to resolve ambiguities at Ka-band in the likely event that stochastic tropospheric fluctuations prevent direct Ka-band ambiguity resolution. All three techniques could help in the case of tracking an object with very poor a priori angular position information. Perhaps the most robust solution would utilize several of these approaches at once: for instance, an array of baselines receiving simultaneous X/Ka downlinks, with widely spaced Ka-band tones for generating a high precision group delay data type.

VI. Summary

A 90-minute observation pass on the DSS 13–DSS 15 baseline has yielded eleven differential phase-delay observables with formal errors of 1 psec and an rms scatter of 10 psec, roughly the level predicted by statistical models of tropospheric fluctuations. These data determined the relative source positions to an accuracy of 60 nrad in one component of sky position. This is the highest angular accuracy achieved to date from observations within a single DSN tracking complex. The other component of source position was not well determined, due to the short observing period. However, similar observations spanning the mutual visibility window for this source would provide comparable accuracy for both components of sky position. Placing a quantitative value on the probability of a cycle error is difficult without a better understanding of the probability distributions of the underlying error sources, although examination of the distribution of phase residuals suggests that the cycle ambiguity resolution was successful.

Developing techniques to ensure highly reliable ambiguity resolution is a prerequisite to incorporating CEI into operational spacecraft tracking. At Ka-band, the few-millimeter level of stochastic tropospheric fluctuations

observed in this experiment would seriously complicate ambiguity resolution. In addition, large uncertainties in a priori source position would also hamper ambiguity resolution. Several techniques have been outlined for using less accurate, but more easily resolved, data types to aid in resolving a higher accuracy observable. Data collected in the last few months and over the coming year should allow some of these techniques to be tested and evaluated.

Acknowledgments

I would like to thank Lyle Skjerve, Ben Johnson, and Earl Lobdell for their invaluable efforts in acquiring these data, George Lutes and Lute Maleki for their assistance in using the fiber-optic link between DSS 13 and DSS 15, Dick Branson and Ojars Sovers for implementing and testing some new features in the MASTERFIT parameter estimation software, and Jim Ulvestad, Bill Folkner, Mark Finger, and Sam Thurman for their comments on a preliminary draft of this article.

References

[1] C. D. Edwards, "Short Baseline Phase Delay Interferometry," *TDA Progress Report 42-91,* vol. July–September 1987, Jet Propulsion Laboratory, Pasadena, California, pp. 46–56, September 15, 1987.

[2] C. D. Edwards, "Angular Navigation on Short Baselines Using Phase Delay Interferometry," *IEEE Transactions on Instrumentation and Measurement*, vol. 38, pp. 665–667, 1989.

[3] R. N. Treuhaft, "Deep Space Tracking in Local Reference Frames," *TDA Progress Report 42-94,* vol. April–June 1988, Jet Propulsion Laboratory, Pasadena, California, pp. 1–15, April 15, 1988.

[4] J. S. Border and R. D. Kahn, "Relative Tracking of Multiple Spacecraft by Interferometry," Paper AAS-89-178, *Proceedings of the AAS/GSFC International Symposium on Orbital Mechanics and Mission Design*, Greenbelt, Maryland, April 1989.

[5] C. D. Edwards, "The Effect of Spatial and Temporal Wet-Troposphere Fluctuations on Connected Element Interferometry," *TDA Progress Report 42-97,* vol. January–March 1989, Jet Propulsion Laboratory, Pasadena, California, pp. 47–57, May 15, 1989.

[6] G. Lutes and A. Kirk, "Reference Frequency Transmission Over Optical Fibers," *TDA Progress Report 42-87,* vol. July–September 1986, Jet Propulsion Laboratory, Pasadena, California, pp. 1–9, September 15, 1986.

[7] B. G. Clark, "The NRAO Tape-Recorder Interferometer System," *Proc. IEEE,* vol. 61, pp. 1242–1248, 1973.

[8] J. B. Thomas, "Interferometry Theory for the Block II Processor," JPL Publication 87-29, Jet Propulsion Laboratory, Pasadena, California, October 15, 1987.

[9] A. E. E. Rogers, "Very Long Baseline Interferometry with Large Effective Bandwidth for Phase-delay Measurements," *Radio Science,* vol. 22, pp. 1239–1247, 1970.

[10] O. J. Sovers and J. L. Fanselow, "Observation Model and Parameter Partials for the JPL VLBI Parameter Estimation Software 'MASTERFIT'-1987," JPL Publication 83-39, Rev. 3, Jet Propulsion Laboratory, Pasadena, California, December 15, 1987.

[11] R. N. Treuhaft and G. E. Lanyi, "The Effect of the Dynamic Wet Troposphere on Radio Interferometric Measurements," *Radio Science,* vol. 22, pp. 251–265, 1987.

[12] J. S. Border and W. M. Folkner, "Differential Spacecraft Tracking by Interferometry," *Proceedings of the CNES International Symposium on Space Dynamics,* Toulouse, France, November 6–10, 1989.

Table 1. Frequency configuration

Channel	DSS 13 frequency, MHz	DSS 15 frequency, MHz	Sideband, upper/lower	Dwell time, sec
1	2304.9999	2305.0001	LSB	0.4
2	2264.9999	2265.0001	USB	0.4
3	2297.9999	2298.0001	LSB	0.4
4	8439.9999	8440.0001	LSB	1.6
5	8399.9999	8400.0001	USB	1.6
6	8432.9999	8433.0001	LSB	1.6

Table 2. The a priori J2000 source positions

Source	Right ascension, h m s	Declination, o ′ ″
3C 84	03 19 48.160328	41 30 42.10581
OE 400	03 03 35.242181	47 16 16.27738

Table 3. Observation sequence

Observation no.	Source name	Start − stop, GMT	Average elevation, deg
1	3C 84	213100 - 213400	56.7
2	OE 400	213442 - 213742	53.2
3	3C 84	213824 - 214124	55.3
4	OE 400	214206 - 214506	51.9
5	3C 84	214542 - 214842	54.9
6	OE 400	214924 - 215224	50.7
7	3C 84	215300 - 215600	52.6
8	OE 400	215642 - 215942	49.5
9[a]	3C 84	220018 - 220318	51.2
10[a]	OE 400	220354 - 220654	48.2
11	3C 84	220730 - 221030	49.9
12	OE 400	221106 - 221406	47.0
13	3C 84	221442 - 221742	48.5
14	OE 400	221818 - 222118	45.8
15	3C 84	222154 - 222454	47.2
16	OE 400	222530 - 222830	44.6
17	3C 84	222906 - 223206	45.9
18	OE 400	223242 - 223542	43.4
19	3C 84	223618 - 223918	44.5
20	OE 400	223954 - 224254	42.2
21	3C 84	224330 - 224630	43.2
22	OE 400	224706 - 225006	40.9
23	3C 84	225042 - 225342	41.9
24	OE 400	225418 - 225718	39.7

[a] These two observations were lost due to a malfunction of the antenna pointing computer at DSS 13. (Observations are grouped in pairs used to form the final differential observables.)

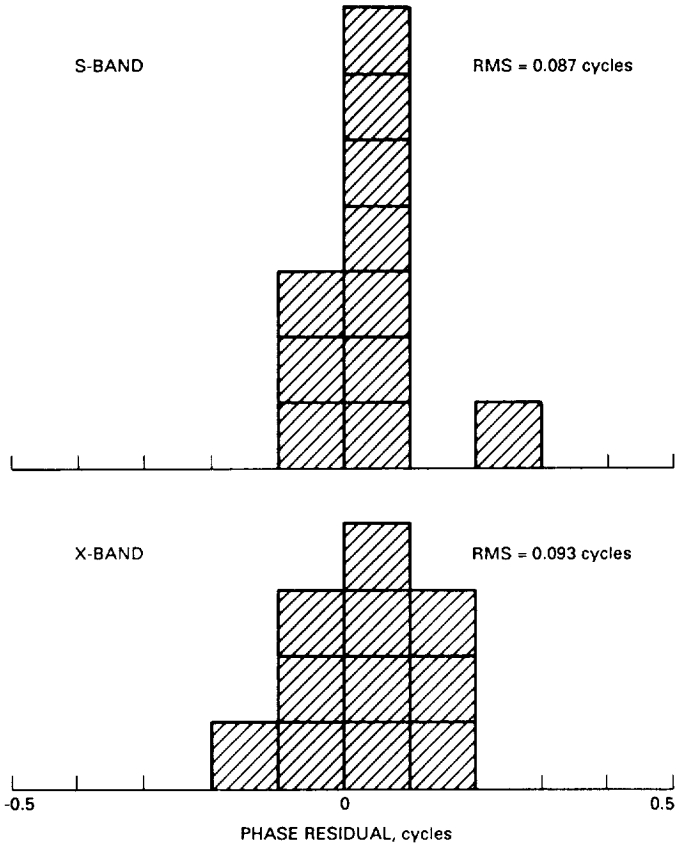

Fig. 1. S-band and X-band phase residuals after ambiguity resolution. The rms width of the distribution is 0.087 cycle at S-band and 0.093 cycle at X-band.

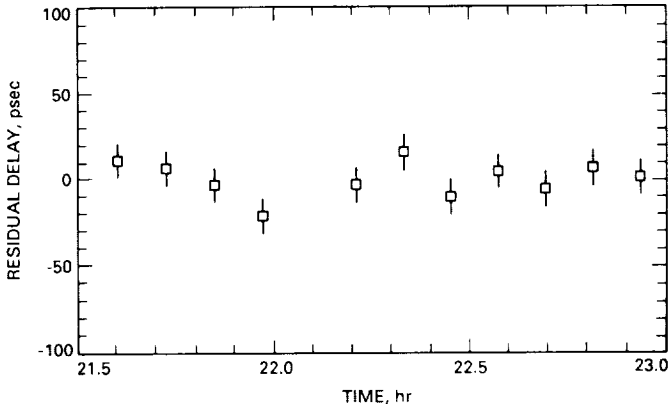

Fig. 2. Final S/X-combined differential phase-delay residuals as a function of time over the 90-minute observation.

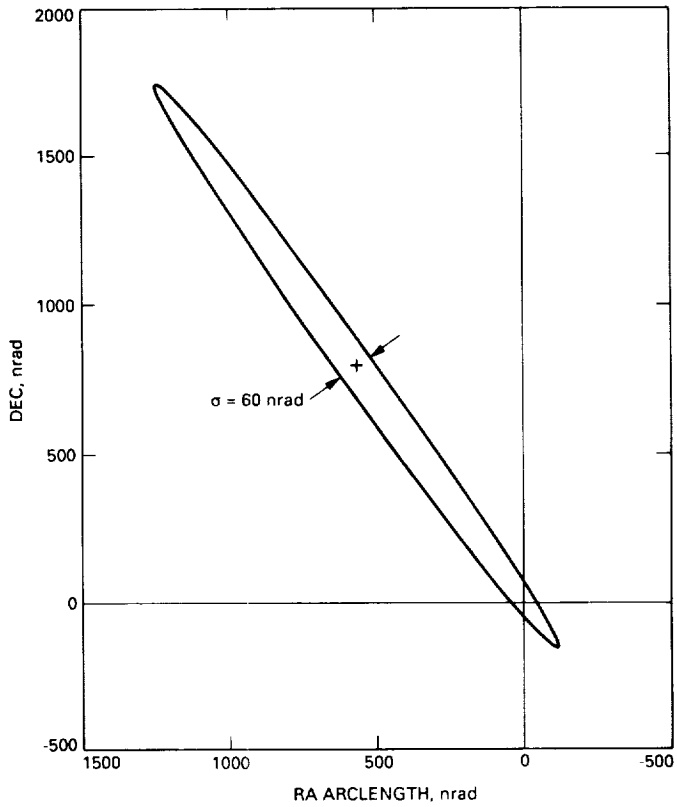

Fig. 3. Estimated source position correction and error ellipse for OE 400, based on a weighted least-squares fit to the phase-delay residuals shown in Fig. 2. The orientation of the ellipse corresponds to the average projected baseline direction over the 90-minute observation period.

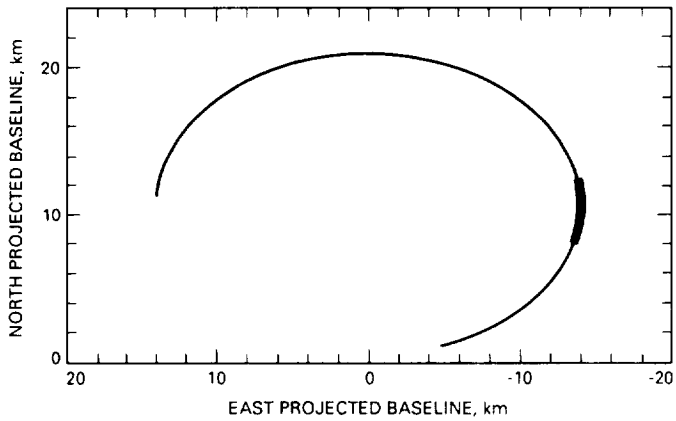

Fig. 4. The projection of the DSS 13–DSS 15 baseline on the plane of the sky, in the direction of the radio source OE 400, over the full mutual visibility window of over 15 hours. The portion of the visibility window represented by the 90-minute observation reported here is shown with a heavier line; during this short period, the projected baseline only rotates through about 10 degrees, and so the resulting position determination is much stronger in one direction on the plane of the sky than in the other.